White Rose Research Online

eprints@whiterose.ac.uk
https://eprints.whiterose.ac.uk
Universities of Leeds, Sheffield and York

Deposited via The University of Sheffield.

White Rose Research Online URL for this paper:
https://eprints.whiterose.ac.uk/id/eprint/147867/

Version: Accepted Version

Article:
Narayanan, A., Mostafavi, M., Pirling, T. et al. (2019) Residual stress in laser cladded rail. Tribology International, 140. 105844. ISSN: 0301-679X

https://doi.org/10.1016/j.triboint.2019.105844

Article available under the terms of the CC-BY-NC-ND licence (https://creativecommons.org/licenses/by-nc-nd/4.0/).

Reuse
This article is distributed under the terms of the Creative Commons Attribution-NonCommercial-NoDerivs (CC BY-NC-ND) licence. This licence only allows you to download this work and share it with others as long as you credit the authors, but you can't change the article in any way or use it commercially. More information and the full terms of the licence here: https://creativecommons.org/licenses/

Takedown
If you consider content in White Rose Research Online to be in breach of UK law, please notify us by emailing eprints@whiterose.ac.uk including the URL of the record and the reason for the withdrawal request.

UNIVERSITY OF LEEDS
University of Sheffield

UNIVERSITY of York

Residual stress in laser cladded rail

A Narayanan[1], M Mostafavi[1], T Pirling[2], S Kabra[3], R Lewis[4], MJ Pavier[1], MJ Peel[1]

1- Department of Mechanical Engineering, University of Bristol, Bristol, UK
2- Institut Laue-Langevin, Grenoble, France
3- ISIS Neutron Source, Rutherford Appleton Laboratory, Didcot, UK
4- Department of Mechanical Engineering, University of Sheffield. Sheffield, UK

Abstract

To improve the fatigue life of components subject to loads with high surface strain gradients, it is possible to coat them with an alloy of higher durability. The present study focuses on the effect of cladding high value track components, made of a standard rail steel UIC 900A/grade 260, with a layer of a premium martensitic stainless steel to reduce wear and fatigue. The laser cladding process inevitably generates residual stresses in the clad and parent metal, which could be detrimental to the integrity of the component. Therefore, measurements to determine the residual stress state of cladded rail were performed using semi-destructive centre-hole and deep hole drilling and non-destructive neutron diffraction techniques. Subsequently, the effects of cycling loading and wear, representative of typical service loads, on the redistribution of the residual stress field were investigated. It was observed that laser cladding causes a triaxial compressive residual stress field in the clad and near the interface and a tensile stress field in the parent material. The stress field is shown to change when the first cycle of load is applied but reaches a steady state after only 10 cycles: After the 10th cycle there is no evidence that the clad continues accumulating strain which could indicate that there is low risk of ratcheting. Wear effect on residual stress redistribution was found to be local on the surface of the specimen only.

1. Introduction

Wheel/rail interface conditions are becoming more severe as contact stresses rise and train speeds increase [1]. There is also a growing level of rail traffic [2]. As a result, more attention is being paid to solutions to increase wheel and rail life. New materials are being developed and new processes including additive manufacturing techniques, such as laser cladding, for adding premium materials to a standard grade substrate to increase rolling contact fatigue (RCF) and wear life. These approaches are preferable to the application of curve lubricants and top of rail friction modifiers which are known to reduce damage levels [3][4][3] as the wayside applicators used require regular maintenance [5].

Coatings are used for many applications where the properties of the surface are required to be different to the bulk material. In large scale industries, coatings are used in various fields from power generation [6–8], transportation [9–11] and healthcare [12,13], but there is no widespread use of such coatings in the railway industry so knowledge of how they behave in the wheel/rail interface is limited.

Recent small and full-scale tests simulating a wheel/rail interface have indicated that cladding of martensitic stainless steel (MSS) and Stellite 6 shows real promise across a wide range of contact conditions (including those relevant for tangent and curved rail and those typical of wheel/switch blade contact) in terms of their wear resistance and suppression of crack initiation [14–17]. Laser cladding shows presents a better option than other similar processes such as arc welding as it produces a finished coating with less porosity and more homogeneity and properties are more easily controlled.

Crack initiation and progression follows a number of stages [18]. Initiation is driven by a ratchetting process; crack growth is then progressed due to contact stresses; finally, cracks can

turn down and develop rapidly due to bending. This can lead to rail breaks if not arrested. Bending tests have been carried out on clad rail specimens [16]. These showed that MSS outperformed standard grade rail. Stellite 6, however, failed prematurely. This was due to some porosity, but may also have been influenced by its tensile residual stress state, which differs from the compressive state in the MSS layer [16].

When it comes off the production line, rail typically has a compressive residual stress. This is beneficial as this has been shown to improve wear and RCF resistance [19,20]. Post manufacturing heat treatment to increase hardness can help increase compressive residual stresses [21]. However, it was found in this work that using 40 seconds cooling rather than 20 seconds reduced the compressive stress reached. Variations in the thermal parameters used in laser cladding could possibly cause similar effects.

As a wheel or rail surface is plastically deformed and work hardened during rolling cycles during the passage of train wheels the compressive residual stress is increased [22]. In wheels, however, high thermal events, for example, tread braking or a wheel slide, can change the residual stress below the surface to tensile [22,23]. The same principle may apply to rail from a wheel slide/spin and lead to crack initiation and squat formation. Laser clad layers have much more tolerance to high heat input from sliding [24] which may help in this regard. It has also been noted that at high contact stresses internal residual tension may develop and cause promote sub-surface fatigue cracking. Coarse microstructures have also been shown to induce tensile residual stress, where finer microstructures remain compressive in rolling-sliding contacts [25]. This should be less of a problem in cladding application but must be considered. Weld repairs (that involve similar thermal processes to cladding) in rail can induce unfavourable residual stress conditions. Optimisation of the application process, however, can ensure that a good level of compressive residual stress is achieved [26].

When implementing new solutions to improve rail life that involve addition of material to the rail (weld repair; cladding etc.), it is clear that residual stresses must be fully characterised understood in order to optimise the material choice/thermal processing parameters to avoid conditions that may lead to delamination/damage. In the case of the clad layer, this could help in reducing the likelihood of damage and in applying multiple layers (to increase depth of material applied), where a tensile residual stress may result in delamination.

Understanding of residual stresses is also important in planning grinding strategies for the clad layers. If sharp radii are left in the contact zone high residual stresses could be generated and lead to sub-surface fatigue being induced [22,27]. Removal of too much material may remove the region of peak compressive residual stress [23].

Residual stresses in rails generally are understood. Residual stresses that are developed in the rail as a result of laser cladding, alter the mean stress of the cyclic bending loads that are endured by tracks. The effects of changing the mean stresses on fatigue life are well established [28] but until the residual stress field in track is measured, it is difficult to estimate its direct effect as high levels of load could result in residual stress redistribution and therefore change of mean stress.

The residual stress fields generated by the cladding of rail have not been investigated previously. In particular, it is not known how the stresses affect the performance of the components subject to cyclic loading [29,30]. Therefore, this study is intended to experimentally measure the residual stresses rail coated using laser cladding. Various semi-destructive and non-destructive techniques such as centre hole drilling, deep hole drilling, and neutron diffraction are used to measure as-cladded residual stress fields. In-situ loading neutron diffraction method was used to monitor the change in the clad residual stress as cyclic bending stress is applied on the clad rail. A through discussion on the uncertainty of measuring residual

stresses with different techniques and different instruments was provided to consolidate the residual stress measurements.

2. Experimental procedures

2.1. Material and specimens

The rail material was pearlitic steel (UIC 900A/grade 260) and the clad material is martensitic steel of composition (0.04% C, 13% Cr, 4.1% Ni, Fe Balanced) [31]. Rail steel Grade 260 has elastic modulus of 207 GPa and a 0.2% proof strength of 470 MPa [32]. The martensitic steel clad material has an elastic modulus 208 GPa and 0.2% proof strength 540 MPa [33].

Schematic of the cladded specimen used in the residual stress measurement programme and its dimensions are shown in Figure 1A. Figure 1B shows the location of various residual stress measurements carried out on the specimen. As Figure 1A shows the clad had been deposited over the upper surface in two passes to a depth of ~2 mm and ground to a nominal thickness of 1.2 mm. Preliminary measurement showed the clad depth varies between 1.1 and 1.3 mm depth. The details of the cladding parameters are the intellectual property of Laser Cladding Ltd., as such, cannot be disclosed. The specimen shown in Figure 1A was 0.5 m long; it was sectioned in half length-wise to create one sample for semi-destructive residual stress measurements (i.e. centre hole drilling and deep hole drilling) and another for non-destructive (i.e. neutron diffraction) in-situ loading measurements. It is assumed that the cladding process was approximately steady-state over the length and as such the stress measurements on the two halves are comparable. The required bending loads were reduced by cutting the bending sample at the half-height. As will be shown later, the stress state is essentially zero by this depth and there is no redistribution of residual stresses as result of half-height cut.

2.2. Semi-destructive Stress Measurements

Semi-destructive techniques for residual stress measurement, unlike non-destructive techniques such as neutron diffraction, rely on mechanical removal of the material. As such, comparison the measurements made using the two types of techniques (semi-destructive and non-destructive) can provide useful insight into their reliability. Here we have used two semi-destructive methods: the incremental centre hole drilling (ICHD) technique, which has low depth penetration but is accurate at the surface, and incremental deep hole drilling (IDHD), which can measure deep into a sample but does not provide reliable data at the surface [34].

ICHD measures in-plane residual stress components by incrementally drilling a hole and measuring the change in surface strain as the stresses redistribute. Reverse calculations are used to determine the initial residual stress state. The formulae and coefficients required for the reverse calculations have been determined by experimental and numerical study and are found in ASTM Standard E837-13a [35] along with detailed guidelines on how to perform the process accurately. Depth resolution is obtained by incrementally increasing the hole depth. ICHD is restricted to near surface measurements although greater depth can be obtained by using a larger diameter drill (albeit at the cost of reduced depth resolution). Here, one measurement was made using a 2 mm diameter drill to a depth of 1 mm in increments of 0.05 mm. In addition, another measurement was carried out using a 4 mm drill to a depth of 2 mm in increments of 0.1 mm. This was to cross the clad/substrate interface. Since the drilling is destructive, measurements were made at two different locations on the centreline of the rail 20-50 mm from the transverse edges (see Figure 1B for the location of the measurements). It is assumed that the cladding process was approximately steady-state over the length of the specimen, the two measurements should be comparable.

IDHD is performed by drilling a pilot hole with a nominal diameter of 1.5 mm through the component and measuring its diameter with an air probe. Stress relief is then applied by

trepanning a concentric ring of 5mm internal diameter around the pilot hole using electron-discharge machining, after which the diameter of the pilot hole is re-measured. The distortion of the pilot hole after trepanning can then be used to calculate the original residual stresses in the material[36]. Previous comparison between the IDHD and neutron diffraction measurements have shown good agreements [34,36–38]. Here, pilot hole measurements have been made at increments of 0.1 mm. The IDHD measurement was done at the same location as the neutron measurements on SALSA at the half-length of the sample (Figure 1A).

2.3. Non-destructive Stress Measurements

Neutron diffraction was used to measure the residual stress non-destructively through the depth of the specimen as well as its variation as a result of applying load. The short duration of the awarded beamtimes necessitated using two different instruments for each part of the experiment. SALSA, at the Institut Laue-Langevin, was used for depth measurement and ENGINX, at ISIS neutron source, Rutherford Appleton Laboratories for in-situ loading measurements. The two instruments have similarities and differences which are high-lighted below.

In both instruments the measurement location is defined by slits and/or collimators on the incident and diffracted beams. Strain in the region that is both exposed to neutrons and visible to the detector is measured (see Figure 2). At a diffraction angle near 90º this results in a near cuboid interaction volume. The direction of the measured strain is determined by the scattering vector, which is the bisector of the incoming and diffracted beams.

All diffraction methods measure stress in a crystalline material by determining the lattice spacing, *d*. The sample is exposed to a beam of neutrons which then scatter from the crystal lattice and interfere resulting in peaks of high intensity that can be measured by a detector. At SALSA a monochromatic neutron beam is used, and diffraction peaks occurs at different angles corresponding to different crystal planes. Only a small portion of the angular range can be sampled by the position sensitive detector so only one reflection is measured. The corresponding plane spacing is obtained by measuring the diffraction angle 2θ and using the Bragg relation $d^{hkl} = \lambda/2\sin\theta$, where (*hkl*) is the Miller indices of the diffraction plane. The (211) plane was used which has a nominal 2θ =83º at a wavelength of 0.15 nm (the wavelength used at SALSA). When a strain is present the lattice spacing shifts and this manifests as a change in 2θ. The strain is calculated via the relation

$$\varepsilon = \frac{d^{hkl} - d_0^{hkl}}{d_o^{hkl}}$$

where $d_0^{hkl}$is the lattice spacing in an otherwise identical sample not subject to a stress and ε is the strain perpendicular to [hkl] plane. d_0^{hkl} can vary due to composition differences and so needs to be measured as a function of depth in clads. Dependency of d_0^{hkl} with chemical composition through the samples depth was identified by making a thin (~2mm) slice of rail and adding comb shape cuts to relieve any remaining macroscopic stresses (Figure 3).

The ENGINX instrument uses a neutron beam with a range of wavelengths from 0.05 – 0.6 nm and a fixed diffraction angle (90º). Neutrons are discriminated by their energy, which manifests as changes in flight time *t* since $d^{hkl} = f(t, \sin\theta)$. In this approach, it is possible to measure multiple (*hkl*) reflections at the same time. Commonly, the unit cell parameter (a in a cubic material like steel) is obtained by simultaneously fitting all reflections to a crystallographic model using GSAS [39]. The strain is then calculated via $\varepsilon = (a - a_0)/a_0$. The same sliced comb shape sample that was used in SALSA was also used in ENGINX to measure a_0, the unstressed unit cell parameter.

Calculations of stress require multiple strain components, so the sample was rotated, and repeat measurements made. It was assumed the principal stress directions aligned with the coordinate system shown in Figure 1 i.e. the obvious sample symmetry. Under these conditions the principle stress components are obtained via

$$\sigma_i = \frac{E^{hkl}}{1+\nu^{hkl}}\left[\varepsilon_i + \frac{\nu^{hkl}}{1-2\nu^{hkl}}(\varepsilon_1+\varepsilon_2+\varepsilon_3)\right]$$

where $E^{hkl}$and $\nu^{hkl}$are plane dependent elastic diffraction and Poisson ratio constants, σ_i $(i = 1,2,3)$ are principle stresses and ε_i $(i = 1,2,3)$ are their corresponding principle strains. For the SALSA experiment, which used the (211) reflection, $E^{hkl} = 225\ GPa$ and $\nu^{hkl} = 0.28$ were calculated using the ISODEC program [40]. For the ISIS experiment, where multiple reflections are used, it is reasonable to use macroscopic elastic constants where $E^{hkl}$is replaced by E=207 GPa and ν^{hkl} by $\nu = 0.3$ [41].

In a clad the interaction volume passes through two interfaces: air/clad and clad/substrate. Diffraction is inherently phase selective so this can lead to partial filling of the volume and spurious strains [42,43]. This is illustrated schematically in Figure 4A. If the volumes are entirely within either clad or substrate the real centre of mass matches the apparent one. If the volume is partially in the air, then there can be no diffraction from part of the volume and centre of mass shifts. This changes the real depth of the measurement but also the diffraction angle - resulting in false strains. A similar effect could happen at the clad/substrate interface. Since the clad and substrate have the same ferritic crystal structure we expect the same diffraction pattern albeit shifted due to differences in chemistry. If the shift is large we might see two peaks and get a false strain from both. Smaller shifts lead to overlaid peaks that are hard to fit with simple functions. Figure 4B shows examples of peaks from the clad, the substrate and on the interface. The martensitic clad has broader peaks than the substrate and this increased the required count times. Fortunately, there is no evidence that the peaks from martensitic and pearlitic steels (i.e. the clad and the rail) are splitting and a Gaussian function appear to appropriately fit the peaks at all depths. Near the surface and the interface the peaks are both notably broader (high σ) and lower intensity (I) than in the substrate, leading to higher uncertainty in lattice parameter and hence strain.

Some caution is needed when evaluating the error in stress. An estimate of the uncertainty in the lattice parameter measurement is derived from the peak fit and this can be readily propagated through the strain and stress calculations. However, a single measured d_0^{hkl} value is used at each depth, so the errors in strain are not independent. Neglecting the error in d_0^{hkl} significantly underestimates the error in stress. Methods are available to account for this (e.g. [42,44,45]). Here we have used the 'uncertainties' python package that propagates all errors through stress calculations [46].

The focus of the SALSA measurements was to quantify the as clad residual stresses as a function of depth from 0.4 mm in the clad to 4 mm in the substrate. Reducing acquisition times was achieved by increasing the size of the interaction volume at depths where spatial resolution was less important starting with 0.6×2×2 mm^3 in the clad to 0.6×10×10 mm^3 in the substrate (see Table 1 for details of the measurements). A small volume was used in the clad, where high stress gradients are expected, and a larger one in the substrate (depth>1.5 mm), where the stress gradient is essentially zero. The stress field was expected to be in-plane biaxial so the interaction volume could be extended in the x or y directions without error. The lattice parameter was measured at 16 locations between 0.4 and 4 mm below the clad surface. Some measurements were made closer to the surface but the strain error introduced by partial filling proved excessive. To calculate stress, three measurements of strain were needed, and this required sample rotation, realignment and repetition of the scan details of which can be found elsewhere [47].

The ENGINX experiments were used to determine how the residual stress changed under cyclic loading. The initial residual stress was measured at three depths in the centre-point of the rail: in the clad (z = 0.7 mm), on the clad-substrate interface (z = 1.2 mm), and in the substrate close to the clad (z = 1.7 mm) to verify the SALSA measurements. ENGINX has two detectors with orthogonal scattering vectors so only two rotations were needed to quantify the stresses from three (longitudinal x, transverse y, and normal z components of strain – see Figure 1). The sample was then subjected to repeated four-point bending, such that the clad layer was in tension. The load was configured to cycle to a maximum surface tensile stress of 250±10 MPa from a minimum of 25 MPa (i.e. R = 0.1). The distance between the inner supports was 120 mm and that of outer supports 200 mm. This load was chosen as it was expected to cause yield at the interface and hence redistribute the residual stress. Measurements were made on the sample before loading and after 1, 10 and 100 cycles. Due to time constraints during the beamtime, only measurement of the longitudinal strain was possible following the set of 100 cycles, so the stress is unknown. The lattice parameter was measured on the same comb shape slice of rail used for the SALSA measurements.

3. Results

3.1. Semi-destructive measurements

The residual stress profiles measured by the two ICHD drill sizes and IDHD are shown in Figure 5. There seems to be a discrepancy between the three measurements although this is likely due to differences in each technique's resolution. In all cases, there is negligible difference between the two in-plane stress components. No shear stress was measured, indicating that the x and y directions of the imposed coordinate system do match the principal axes. The ICHD measurement with the small (2mm) drill shows nearly zero in-plane stress at the surface, which increases to a compressive stress greater than -700 MPa at 0.8 mm depth. The stress then reduces slightly nearer the interface. The ICHD with the larger drill can measure deeper, indicating that the stress tends towards zero in the substrate. However, this measurement does not show the same magnitude of compressive stress in the clad. Most likely, the differences arise from the reduced spatial resolution of the larger drill, where an averaging effect means the gradients are missed. The inability of semi-destructive techniques in measuring steep stress gradients near the interfaces has been seen and discussed by other research's [48]. The IDHD measurements also show the stress tending towards zero in the substrate and the stress gradient is effectively zero by 4mm depth. The stresses in the clad, while also compressive, are rather lower than both ICHD measurements. There is a minor local drop at 0.9 mm depth, but, as with the larger ICHD drill, it appears the gradients are too strong to capture with this technique. Further, the surface stresses are not expected to be reliable due to the lack of sensitivity of IDHD near a surface [49].

These stress profiles measured by semi-destructive were used to plan the time constrained neutron measurements e.g. there is no need to measure at depths below 4mm and the greatest uncertainty is in the clad where resolution is required.

3.2. Non-destructive measurement

The lattice spacing was measured in the stress-free d_0 sample as a function of depth below the clad surface (i.e. along the normal z direction). In all cases, the lattice parameter was measured in the x-direction since in this geometry the value is less sensitive to partial filling. Figure 6 shows the measured lattice spacing with depth as measured on the SALSA instrument. Unsurprisingly, it is constant in the substrate (only a portion is shown here, although measurements were taken down to 19 mm depth). The lattice parameter increases rapidly near the interface and in the clad. The variation is smooth across the interface, which can be mostly attributed to averaging over the interaction volume. A simple prediction is shown where a step

function is used for the assumed d_0^{hkl} in the clad and substrate (i.e. no mixing at the interface) and smoothing derived by the weighted average lattice parameter within the interaction volume.

Experimentally, it was difficult to ensure the location of the measurements in the rail perfectly align with those in the unstressed sample. Therefore, values for d_0^{hkl}, and its uncertainty, were linearly interpolated. It was assumed the uncertainty was depth dependent (it is observably greater in the clad than the substrate) and that interpolated values are representative of the real error. For the substrate (i.e. $z > 1.6$ mm), an average was taken over the range 1.6-19 mm.

Figure 7 shows the residual stresses in the principal directions as a function of depth below the clad surface as measured by SALSA instrument. While measurements were attempted closer than 0.4 mm from the surface, these exhibited large uncertainties and physically implausible values. Examination of the spectra suggests this is primarily a result of poor counting statistics rather than partial filling of the interaction volume. The in-plane stresses (σ_x, σ_y) are essentially equi-biaxial similar to that measured by the semi-destructive techniques. The stresses are slightly compressive near the surface and increase in magnitude to reach a strongly compressive stress of -600 MPa at 1mm depth. The interface is nominally at 1.2 mm depth, although it oscillates between 1.1 and 1.3 mm, suggesting the peak stresses are in the martensitic clad, which exists in a state of high compression. The stress components reduce rapidly at greater depths and reach zero by 1.4 mm depth. A small maximum in tensile stress is seen at 1.5 mm depth and then the stresses settle to 50 MPa by 3 mm depth.

The out-of-plane stress component (σ_z) has the same form, albeit less compressive in the clad. Stress in this direction should tend towards zero at the surface which seems to be satisfied in Figure 7 given the error bars. Near the nominal interface, the stress is essentially hydrostatic in character. The error bars, arising from uncertainty in peak position (for both the measurements and the unstressed lattice parameter), are small in the substrate (1 std ~35 MPa) but considerably larger in the clad (1 std ~ 150 MPa). This occurs through a combination of worse counting statistics, due to the smaller interaction volume, and wider peak width in the martensite clad. There is no discontinuity in stress at the nominal interface, which confirms the assumption that partial filling of the interaction volume by each material does not lead to spurious strain shifts.

The stress was only measured at three locations using the ENGINX instrument i.e. in the clad, the substrate and at the interface. Comparing the initial stress components before loading, it was observed that the ENGINX measurements are consistently much more compressive than the SALSA data, showing a maximum compressive stress in excess of -800 MPa which is physically impossible as the material ultimate strength is -700 MPa difficult to reconcile with the expected boundary condition at the surface (i.e. zero stress). It was therefore concluded that the d0 measurements carried out at ENGINX were erroneous. Moving all the stress values up by 350 MPa to match the as-clad residual stress measurement in the clad between ENGINX and SALSA measurement results in much more agreement between the results obtained at the two instruments as shown in Figure 8.

The effect of cyclic loading on the redistribution of residual stress is shown in Figure 9. It can be seen that cycling does alter the stress, although the change is not large relative to the uncertainty of the measurements. The shift is greatest in the clad and negligible in the substrate. Surprisingly, considering the initially compressive stress state and tensile cyclic stress, the shift is towards greater compression after cycling. The greatest change occurs in longitudinal direction (σ_x) during the first loading cycle with the stress changing by approximately -150 MPa. Subsequent cycles have negligible effect as any change is well within error bar limits. In the transverse direction σ_y, the major change occurs in the clad between 1 cycle and 10 cycles of loading and is of comparable magnitude (~130MPa).

The sample was also loaded for 100 cycles, although time limitations meant that it was only possible to obtain a set of measurements in the longitudinal direction. These strains alone cannot be converted to a stress tensor. However, it could be assumed that the redistribution of the strain components that were not measured, follow the same trend as previous loadings with a magnitude estimated from the longitudinal component that was measured. Such assumption results in a stress field within the error bars of the stress field measured after10 cycles. This demonstrates that most of the change occurs after the first cycle. The additional cycles after the first cycle caused almost no change in strain. This can be seen clearly in Figure 10 which shows the evolution of measured longitudinal strain component as function depth in as-clad condition and after 1, 10, and 100 cycles of loading.

4. Discussion

The residual stress field arising from cladding process of a rail and its redistribution as a result of cyclic loading has been characterised in this work comprehensively. Using various semi-destructive and none-destructive methods (at two different instruments) to measure the residual stresses has the added benefit of exploring the strengths and weaknesses of each technique. It might be expected the methods are complementary each other but there are multiple sources of uncertainty and it may not be always possible to adequately resolve any discrepancies. If the longitudinal stress component taken, for example, the values measured by all the techniques are in general agreement as they all show compressive stresses within the clad that reach a maximum at a depth just below the nominal interface. The agreement between various techniques differ at different measurement points. For example, the IDHD agrees with the SALSA data in the substrate (i.e. both indicate effectively zero longitudinal stress) but has poor agreement in the clad. This is expected as IDHD is known to be poor near the surface due to challenges in accurate hole drilling and measuring. The ICHD (2mm) and SALSA data have excellent agreement with respect to the peak compressive stress but they each appear to be offset in depth by around 0.2 mm. As mentioned above, the ENGINX data is in good agreement with the SALSA data from the point of view of changes in stress from point to point, but there is poor agreement between the absolute value of stress due to the erroneous d0 at ENGINX. This is corrected by shifting all the stress components up by a uniform value to match one measurement point between SALSA and ENGINX confirmed by the ICHD measurement.

These issues highlight a problem and contradiction in using multiple measurement methods for residual stress. It is desirable to do so, since each method is susceptible to errors and uncertainties, and using several techniques will make this clear. However, rationalising these differences is challenging. An attempt of pulling all easements together is shown in Figure 11. In this figure the ICHD (2mm) data is shifted in depth by 0.2 mm. The rationale is that the interface depth varies between 1 and 1.4 mm across the surface and the ICHD measurements were done in a different location to the SALSA and IDHD measurements. After this shift, there is an excellent agreement between the two datasets of semi-destructive and non-destructive measurements. The IDHD measurement has simply been restricted to the substrate where it is expected to give valid data. While the ICHD data is shifted in depth, which may be due to changes in interface depth with position, there was no need to shift the ENGINX data to different depths despite this measurement occurring at an entirely different location to the SALSA/IDHD data.

Beyond a comparison of the different techniques, the data is important in and of itself. The cladding possesses a compressive stress state of relatively high magnitude, while the substrate is moderately tensile in nature. This is may have a positive effect on the fatigue behaviour of the rail as a compressive residual stress reduces the peak tensile stress experienced by the rail although it can have a negative effect on its rolling cycle fatigue as it algebraically increases the compressive stress arising from rail-wheel interaction [9]. As the clad is made of a

martensitic steel, it is likely that the volume changes associated with the transformation into martensite has caused the compressive residual stresses, supporting previous research [50]. There is evidence that suggests an increase in magnitude of compressive residual stresses can improve fatigue resistance by increasing the number of cycles before cracks start forming [51]. In addition, it may provide more resistance to damage formation [52]. This supports an observation by Ringsberg, where a clad of one variety remained undamaged but ended up delaminating from the substrate [9] although other work by Niederhauser and Karlsson shows no cracking at the interface and a strong bond after fatigue tests [53]. In addition, research by Sun [54] has shown reduced performance in fatigue loaded specimens where the clad has a compressive residual stress compared to an untreated substrate material, however this was on tensile fatigue specimens and may not be representative of the loading situation on a real rail track. Nevertheless, it is important to realise that even if this particular clad material reduces the risk of one mode of failure, it may enhance a different mode of failure.

Work was performed to verify the response of the residual stress state in cladded rail to a cyclic, four-point bend load. Results have suggested that within the first 10 cycles, the stresses within the rail reach a steady state. Most change was experienced within the clad, which is expected as it sees the highest magnitude of applied stress superimposed on to the residual stresses. Furthermore, in the longitudinal direction there was the greatest change in stress in the first cycle, with subsequent cycles showing a little further change although well within the error bounds. A comparison of strain measured in this direction after the 100th cycle displays no change in strain and hence it can be concluded that steady state has been reached.

5. Conclusion

Residual stresses have been measured in rail coated using laser cladding to characterise the cladding. Measurements were made using neutron diffraction, incremental centre-hole drilling (ICHD) and deep-hole drilling (DHD) to assess their appropriateness for use on clad components of this kind. It was concluded that:

- Caution is needed when combining results of multiple methods. Unless there is considerable overlap between location of measurements from different techniques, it would not be obvious how entirely independent measured residual stresses can be combined to get the full picture.
- ICHD measurements with 2mm diameter drill had excellent agreement with neutron measurements. While ICHD with a larger diameter hole (4mm diameter) may enable deeper measurements to be made, it comes at the expense of capturing detail such as minima and maxima especially in clads where there is significant strain gradients.
- Neutron diffraction measurements can be made with a high level of success in clad components as partial filling of the gauge volume may not be significant provided the two materials either side of the interface are of similar crystallographic structures.
- The proposed martensitic steel used to clad the rail has a compressive residual stress induced in it by the cladding process which suggest this may have a beneficial effect on the rail fatigue performance. However, the stress state at the interface is triaxial in nature and therefore it is necessary to consider other modes of damage such as delamination at the clad-substrate interface
- Measurements made on rail samples that have been subject to cyclic four-point bending suggest that the residual stress state does redistribute as result of service loading but reaches a steady state after a low number of cycles and steady accumulation of strain with each cycle does not occur with this combination of materials.

Acknowledgements

The authors would like to thank Institut Laue-Langevin and Rutherford Appleton Laboratories for the use of their instrumentation. In addition, Dr Kiranmayi Abburi Venkata, Andrew James, Anthony Reid and Nader Zenturi are all acknowledged for their assistance in performing diffraction experiments. We acknowledge the funding through EPSRC via Rail-energy knowledge exchange on emerging materials (ALCHEMy) grant number EP/M023044/1.

References

[1] M. Stanca, A. Stefanini, R. Gallo, Development of an Integrated Design Methodology for a New Generation of High Performance Rail Wheelsets, in: Proc. 16th Eur. MDI User Conf., Berchtesgaden, Germany, 2001.

[2] National Travel Survey: England 2017, 2018.

[3] C. Hardwick, R. Lewis, R. Stock, The effects of friction management materials on rail with pre existing rcf surface damage, Wear. 384–385 (2017) 50–60. doi:10.1016/J.WEAR.2017.04.016.

[4] L. Buckley-Johnstone, M. Harmon, R. Lewis, C. Hardwick, R. Stock, A Comparison of Friction Modifier Performance using Two Laboratory Scale Tests, Proc. Inst. Mech. Eng. Part F J. Rail Rapid Transit. IN PRESS (2018).

[5] P. Clayton, Tribological aspects of wheel-rail contact: a review of recent experimental research, Wear. 191 (1996) 170–183. doi:10.1016/0043-1648(95)06651-9.

[6] J. Katsuyama, H. Nishikawa, M. Udagawa, M. Nakamura, K. Onizawa, Assessment of Residual Stress Due to Overlay-Welded Cladding and Structural Integrity of a Reactor Pressure Vessel, J. Press. Vessel Technol. 135 (2013) 51402–51409. http://dx.doi.org/10.1115/1.4024617.

[7] D. Wang, Q. Hu, X. Zeng, Residual stress and cracking behaviors of Cr13Ni5Si2 based composite coatings prepared by laser-induction hybrid cladding, Surf. Coatings Technol. 274 (2015) 51–59. doi:10.1016/J.SURFCOAT.2015.04.035.

[8] R. Ghafouri-Azar, J. Mostaghimi, S. Chandra, Modeling development of residual stresses in thermal spray coatings, Comput. Mater. Sci. 35 (2006) 13–26. doi:10.1016/J.COMMATSCI.2005.02.007.

[9] J.W. Ringsberg, F.J. Franklin, B.L. Josefson, A. Kapoor, J.C.O. Nielsen, Fatigue evaluation of surface coated railway rails using shakedown theory, finite element calculations, and lab and field trials, Int. J. Fatigue. 27 (2005) 680–694. doi:10.1016/J.IJFATIGUE.2004.11.002.

[10] J.A.M. de Camargo, H.J. Cornelis, V.M.O.H. Cioffi, M.Y.P. Costa, Coating residual stress effects on fatigue performance of 7050-T7451 aluminum alloy, Surf. Coatings Technol. 201 (2007) 9448–9455. doi:10.1016/J.SURFCOAT.2007.03.032.

[11] J. Lawal, P. Kiryukhantsev-Korneev, A. Matthews, A. Leyland, Mechanical properties and abrasive wear behaviour of Al-based PVD amorphous/nanostructured coatings, Surf. Coatings Technol. 310 (2017) 59–69. doi:10.1016/J.SURFCOAT.2016.12.031.

[12] A.T. Qureshi, W.T. Monroe, M.J. Lopez, M.E. Janes, V. Dasa, S. Park, A. Amirsadeghi, D.J. Hayes, Biocompatible/bioabsorbable silver nanocomposite coatings, J. Appl. Polym. Sci. 120 (2011) 3042–3053. doi:10.1002/app.33481.

[13] G. Ramírez, S.E. Rodil, H. Arzate, S. Muhl, J.J. Olaya, Niobium based coatings for dental implants, Appl. Surf. Sci. 257 (2011) 2555–2559.

doi:10.1016/J.APSUSC.2010.10.021.

[14] S.R. Lewis, R. Lewis, D.I. Fletcher, Assessment of laser cladding as an option for repairing/enhancing rails, Wear. 330–331 (2015) 581–591. doi:10.1016/J.WEAR.2015.02.027.

[15] S.R. Lewis, S. Fretwell-Smith, P.S. Goodwin, L. Smith, R. Lewis, M. Aslam, D.I. Fletcher, K. Murray, R. Lambert, Improving rail wear and RCF performance using laser cladding, Wear. 366–367 (2016) 268–278. doi:10.1016/J.WEAR.2016.05.011.

[16] S.R. Lewis, R. Lewis, P.S. Goodwin, S. Fretwell-Smith, D.I. Fletcher, K. Murray, J. Jaiswal, Full-scale testing of laser clad railway track; Case study – Testing for wear, bend fatigue and insulated block joint lipping integrity, Wear. 376–377 (2017) 1930–1937. doi:10.1016/J.WEAR.2017.02.023.

[17] P. Lu, S. Lewis, S. Fretwell-Smith, D. Fletcher, R. Lewis, Laser Cladding of Rail; the Effects of Depositing Material on Lower Rail Grades, in: 10th Int. Conf. Contact Mech. Wear Rail/Wheel Syst., Delft, The Netherlands, 2018.

[18] A. Kapoor, D. Fletcher, F. Franklin, The Role of Wear in Enhancing Rail Life, in: Proc. 29th Leeds-Lyon Symp. Tribol., 2003: pp. 331–340.

[19] R. Halama, M. Šofer, J. Rojiček, F. Fojtik, K. Kolařik, A Method for Predicting Ratcheting and Wear in Rolling Contact Fatigue taking Techological Residual Stresses into Condiertation, Teh. Vjesn. 24 (2017) 7–14.

[20] S.S. Creţu, N.G. Popinceanu, The influence of residual stresses induced by plastic deformation on rolling contact fatigue, Wear. 105 (1985) 153–170. doi:10.1016/0043-1648(85)90022-5.

[21] M.E. Turan, S. Ozcelik, F. Husem, H. Ahlatci, Y. Sun, I. Tozlu, The effect of head hardening process on the residual stress of rails, Proc. Inst. Mech. Eng. Part F J. Rail Rapid Transit. 232 (2016) 589–595. doi:10.1177/0954409716679450.

[22] O. Orringer, W.R. Paxton, D.E. Gray, P.K. Raj, Residual stress and its consequences on both sides of the wheel-rail interface, Wear. 191 (1996) 25–34. doi:10.1016/0043-1648(95)06674-8.

[23] J.W. Seo, B.C. Goo, J.B. Choi, Y.J. Kim, Effects of metal removal and residual stress on the contact fatigue life of railway wheels, Int. J. Fatigue. 30 (2008) 2021–2029. doi:10.1016/J.IJFATIGUE.2007.12.003.

[24] P. Christoforou, S. Lewis, D. Fletcher, R. Lewis, Benchmarking of Premium Rail Material Wear, in: 10th Int. Conf. Contact Mech. Wear Rail/Wheel Syst., Delft, The Netherlands, 2018.

[25] M. Paladugu, R.S. Hyde, Influence of microstructure on retained austenite and residual stress changes under rolling contact fatigue in mixed lubrication conditions, Wear. 406–407 (2018) 84–91. doi:10.1016/J.WEAR.2018.04.002.

[26] J. Hu, L. Du, H. Xie, F. Dong, R.D.K. Misra, Effect of weld peak temperature on the microstructure , hardness , and transformation kinetics of simulated heat affected zone of hot rolled ultra-low carbon high strength Ti – Mo ferritic steel, 60 (2014) 302–309.

[27] T.N. Farris, Effect of overlapping wheel passages on residual stress in rail corners, Wear. 191 (1996) 226–236. doi:10.1016/0043-1648(95)06724-8.

[28] K. Walker, The effect of stress ratio during crack propagation and fatigue for 2024-T3 and 7076-T6 aluminum, in: M. Rosenfeld (Ed.), Eff. Environ. Complex Load Hist. Fatigue Life, STP462, ASTM International, West Conshohocken, PA, 2970: pp. 1–14.

[29] H. Köhler, R. Rajput, P. Khazan, J.R. Kornmeier, On the Influence of Laser Cladding and Post-processing Strategies on Residual Stresses in Steel Specimens, Phys. Procedia. 56 (2014) 250–261. doi:10.1016/J.PHPRO.2014.08.169.

[30] H. Köhler, K. Partes, J.R. Kornmeier, F. Vollertsen, Residual Stresses in Steel Specimens Induced by Laser Cladding and their Effect on Fatigue Strength, Phys. Procedia. 39 (2012) 354–361. doi:10.1016/J.PHPRO.2012.10.048.

[31] R260 properties, 2016.

[32] A. Mazzù, M. Faccoli, M. Lancini, C. Petrogalli, D. Nélias, A. Ghidini, A Procedure for Wheel and Rail Steels Characterization in Rolling Contact, in: Proc. Second Int. Conf. Railw. Technol. Res. Dev. Maint., 2014.

[33] M. Shahanur Hasan, M. Abdul Mazid, R.E. Clegg, The Basics of Stellites in Machining Perspective, Int. J. Eng. Mater. Manuf. 1 (2016) 35–50.

[34] R.H. Leggatt, D.J. Smith, S.D. Smith, F. Faure, Development and experimental validation of the deep hole method for residual stress measurement, J. Strain Anal. Eng. Des. 31 (1996) 177–186. doi:10.1243/03093247V313177.

[35] ASTM International, ASTM E837-13a Standard Test Method for Determining Residual Stresses by the Hole-Drilling Strain-Gage Method, (2013).

[36] D.J. Smith, Deep Hole Drilling, in: G.S. Schajer (Ed.), Pract. Residual Stress Meas. Methods, John Wiley & Sons, Ltd, 2013: pp. 65–87.

[37] W. Woo, G.B. An, E.J. Kingston, A.T. DeWald, D.J. Smith, M.R. Hill, Through-thickness distributions of residual stresses in two extreme heat-input thick welds: A neutron diffraction, contour method and deep hole drilling study, Acta Mater. 61 (2013) 3564–3574. doi:10.1016/J.ACTAMAT.2013.02.034.

[38] A.H. Mahmoudi, S. Hossain, C.E. Truman, D.J. Smith, M.J. Pavier, A New Procedure to Measure Near Yield Residual Stresses Using the Deep Hole Drilling Technique, Exp. Mech. 49 (2009) 595–604. doi:10.1007/s11340-008-9164-y.

[39] A.C. Larson, R.B. Von Dreele, General Structure Analysis System (GSAS), 2000.

[40] T. Gnäupel-Herold, ISODEC: software for calculating diffraction elastic constants, J. Appl. Crystallogr. 45 (2012) 573–574.

[41] M.R. Daymond, The determination of a continuum mechanics equivalent elastic strain from the analysis of multiple diffraction peaks, J. Appl. Phys. 96 (2004) 4263–4272.

[42] M.E. Fitzpatrick, A. Lodini, Analysis of Residual Stress by Diffraction using Neutron and Synchrotron Radiation, CRC Press, 2003.

[43] X.-L. Wang, S. Spooner, C.R. Hubbard, Theory of the Peak Shift Anomaly due to Partial Burial of the Sampling Volume in Neutron Diffraction Residual Stress Measurements, J. Appl. Crystallogr. 31 (2007) 52–59. doi:10.1107/S0021889897008261.

[44] M. Hutchings, P. Withers, T. Holden, T. Lorentzen, Introduction to the Characterization of Residual Stress by Neutron Diffraction, CRC Press, 2005.

[45] M.T. Hutchings, A.D. Krawitz, Measurement of Residual and Applied Stress Using Neutron Diffraction, Springer Science & Business Media, 2012.

[46] E.O. Lebigot, uncertainties Python package, (2018).

[47] P.J. Withers, H.K.D.H. Bhadeshia, Residual stress. Part 1 – Measurement techniques, Mater. Sci. Technol. 17 (2001) 355–365. doi:10.1179/026708301101509980.

[48] N. Naveed, F. Hosseinzadeh, J. Kowal, Residual Stress Measurement in a Stainless Steel Clad Ferritic Plate Using the Contour Method, in: ASME. Press. Vessel. Pip. Conf. Vol. 5 High-Pressure Technol., 2013: p. V005T11A006.

[49] Y. Javadi, M.C. Smith, K. Abburi Venkata, N. Naveed, A.N. Forsey, J.A. Francis, R.A. Ainsworth, C.E. Truman, D.J. Smith, F. Hosseinzadeh, S. Gungor, P.J. Bouchard, H.C. Dey, A.K. Bhaduri, S. Mahadevan, Residual stress measurement round robin on an electron beam welded joint between austenitic stainless steel 316L(N) and ferritic steel P91, Int. J. Press. Vessel. Pip. 154 (2017) 41–57. doi:10.1016/J.IJPVP.2017.06.002.

[50] S.K. Koh, R.I. Stephens, MEAN STRESS EFFECTS ON LOW CYCLE FATIGUE FOR A HIGH STRENGTH STEEL, Fatigue Fract. Eng. Mater. Struct. 14 (2018) 413–428. doi:10.1111/j.1460-2695.1991.tb00672.x.

[51] R.T.. McGrann, D.. Greving, J.. Shadley, E.. Rybicki, T.. Kruecke, B.. Bodger, The effect of coating residual stress on the fatigue life of thermal spray-coated steel and aluminum, Surf. Coatings Technol. 108–109 (1998) 59–64. doi:10.1016/S0257-8972(98)00665-3.

[52] M.S. Ahmed, Z. Zhou, P. Munroe, L.K.Y. Li, Z. Xie, Control of the damage resistance of nanocomposite TiSiN coatings on steels: Roles of residual stress, Thin Solid Films. 519 (2011) 5007–5012. doi:10.1016/J.TSF.2011.01.070.

[53] S. Niederhauser, B. Karlsson, Fatigue behaviour of Co–Cr laser cladded steel plates for railway applications, Wear. 258 (2005) 1156–1164. doi:10.1016/J.WEAR.2004.03.026.

[54] S. Da Sun, Q. Liu, M. Brandt, V. Luzin, R. Cottam, M. Janardhana, G. Clark, Effect of laser clad repair on the fatigue behaviour of ultra-high strength AISI 4340 steel, Mater. Sci. Eng. A. 606 (2014) 46–57. doi:10.1016/J.MSEA.2014.03.077.

Tables

Instrument	Location	Depth (mm)	Measurement Direction	Interaction volume (mm)	
				Width/depth	Height
SALSA	d0 (all)	0.4-1.4	x		2
	Clad	0.4-1.4	x, z	0.6	10
	Clad	0.4-1.4	y		10
	d0 (all)	1.4-19	x		2
	Substrate	1.4-4	x, z	2	10
	Substrate	1.4-4	y		20
ENGINX	d0	0.7, 1.2, 1.7	x		2
	Clad	0.7			
	Interface	1.2	x, z	0.5	20
	Substrate	1.7			
	Clad	0.7			
	Interface	1.2	y		10
	Substrate	1.7			

Table 1 - Summary of neutron diffraction scans, including direction of measurement and the dimensions of the interaction volume. Each change in width/depth required a new d0 scan. This is not required for changes in height.

Figures

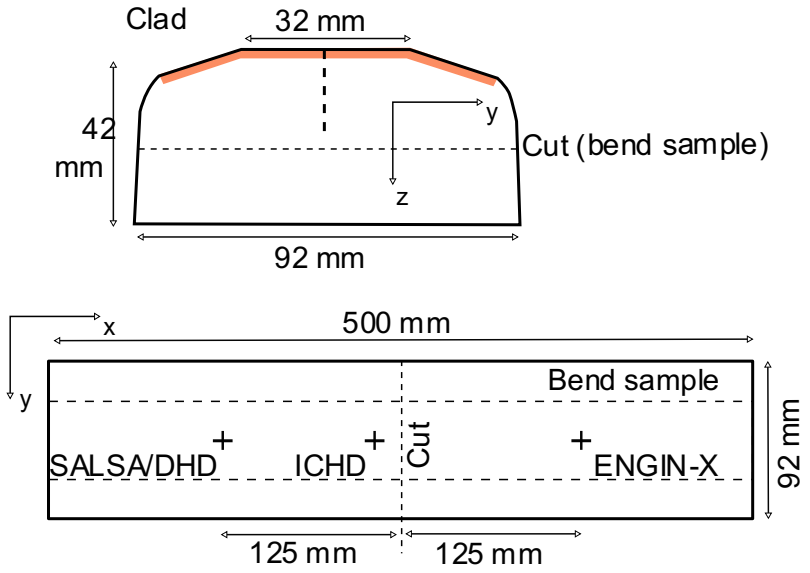

Figure 1 – Schematic of the tested specimens showing the salient dimensions, the location of the clad and the coordinate system used. The bend sample used on ENGINX was reduced in thickness to reduce the required bend loads.

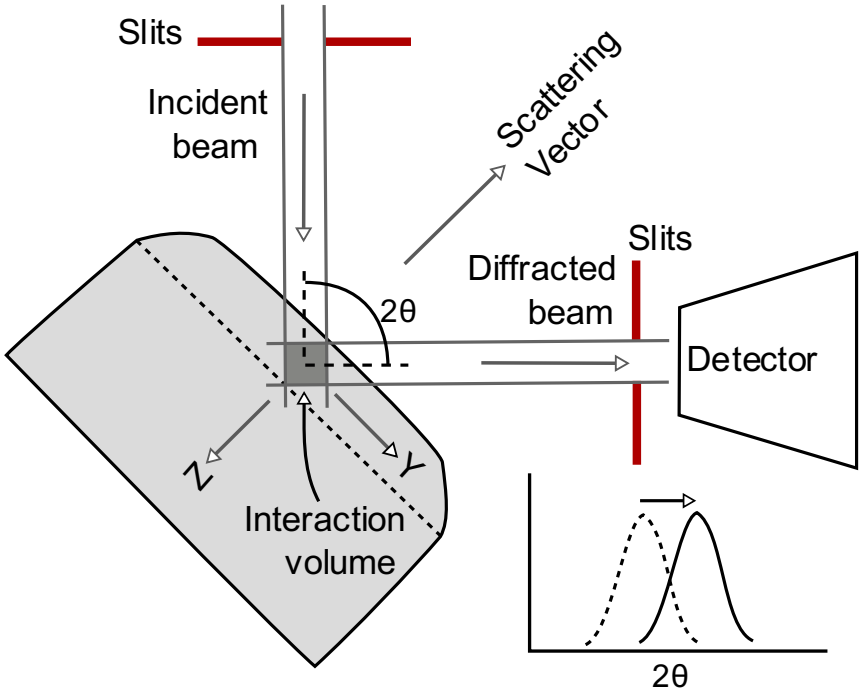

Figure 2 – Schematic of the diffraction setup on the SALSA beamline. The measurement volume is defined by the slit system, while the measurement direction (scattering vector) bisects the incoming and diffracted beams. Different directions are measured by rotating the sample such that the scattering vector is parallel to different axes in the coordinate system. Strain in the sample causes a shift in the measured peak.

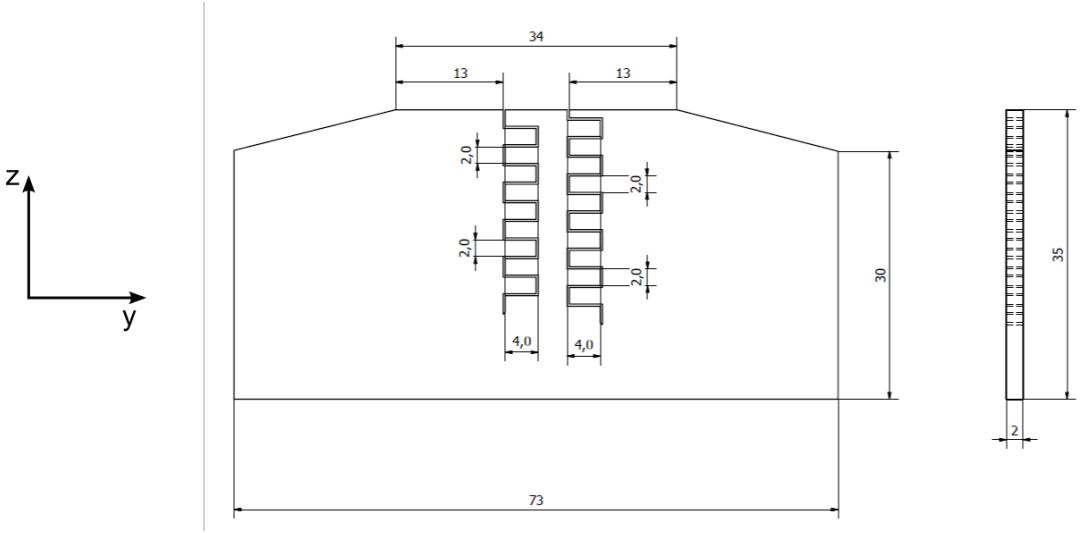

Figure 3 – Geometry of the sample from which the stress-free lattice spacing (d_0) is measured. The low thickness and the teeth should ensure most long-range stress is relaxed.

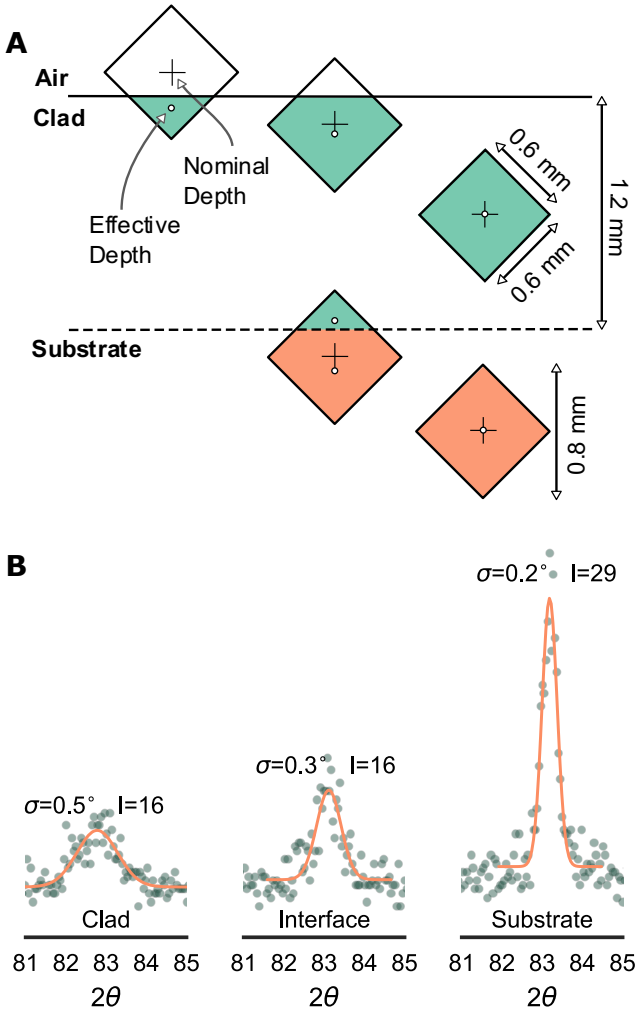

Figure 4 – A) Schematic illustrating partial filling of the measurement volume. The volumes on the right are fully immersed in either clad or substrate and do not lead to spurious strain. The others are partially filled and so the real depth will be different to the apparent depth. B) Examples of peaks from the clad, substrate and the interface demonstrating no evidence of an interface effect from sampling two different alloys (i.e. the peaks are Gaussian in character and symmetrical).

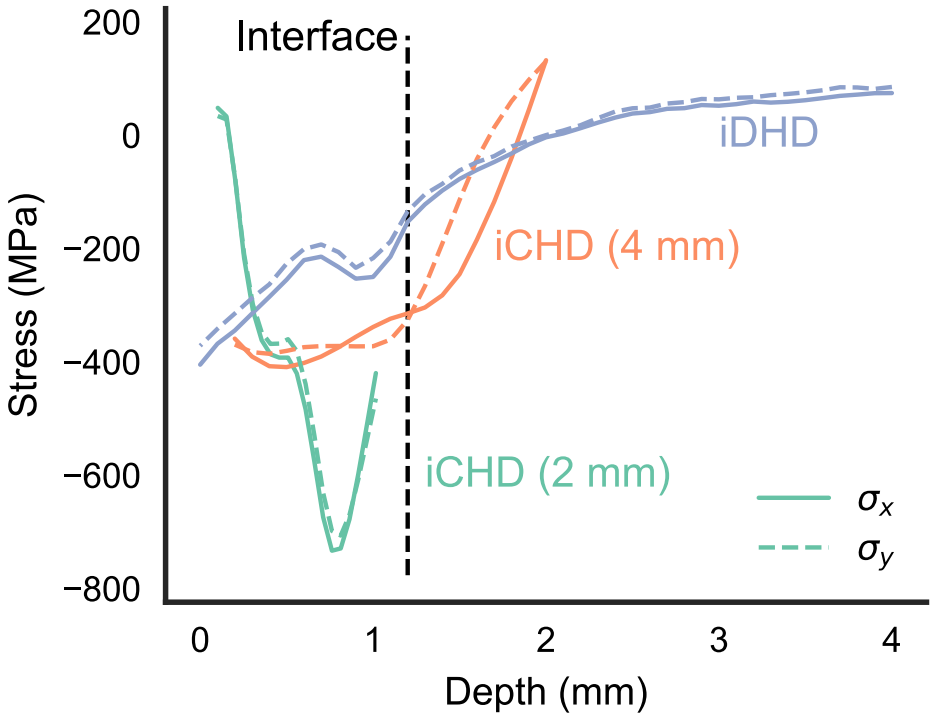

Figure 5 – Residual stress with depth below the clad surface measured using ICHD to a depth of 1 mm using 2 mm hole, ICHD to a depth of 2 mm using 4 mm hole and IDHD to a depth of 4 mm. The nominal depth of the clad is marked. The longitudinal (σ_x) and transverse (σ_y) stress components are indicated by solid and dashed lines, respectively, and it is clear the in-plane stress field is uniform.

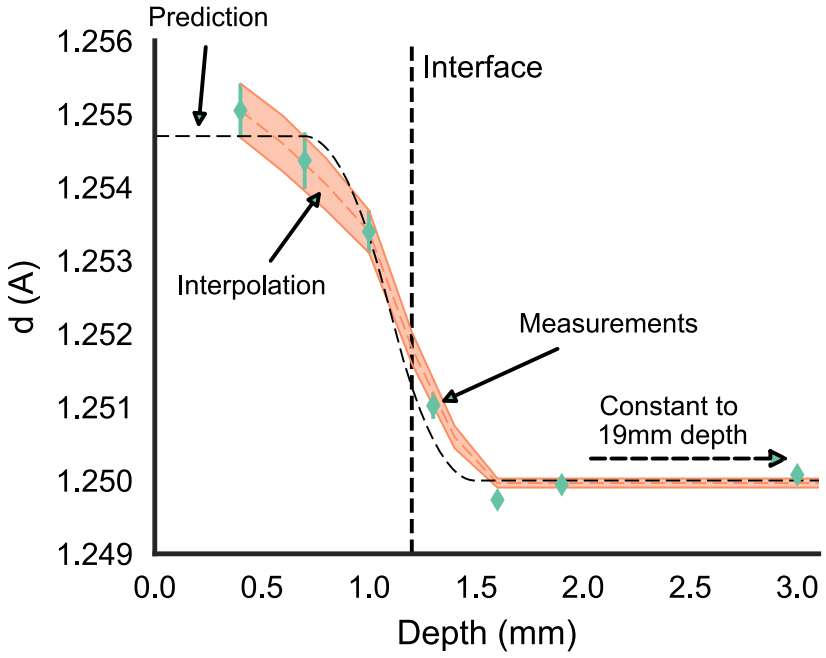

Figure 6 – The unstrained lattice parameter used for the strain calculation on SALSA. Measurements were made on the comb sample and only used fully immersed gauge volumes. Mapping on to the locations measured in the rail sample required interpolation. Spline interpolation was used in the clad while material deeper than 1.5 mm was assigned an average value from the substrate. Both the value and uncertainty were interpolated. The prediction is based on convolution of the sampling volume with a step function for d_0 at the interface.

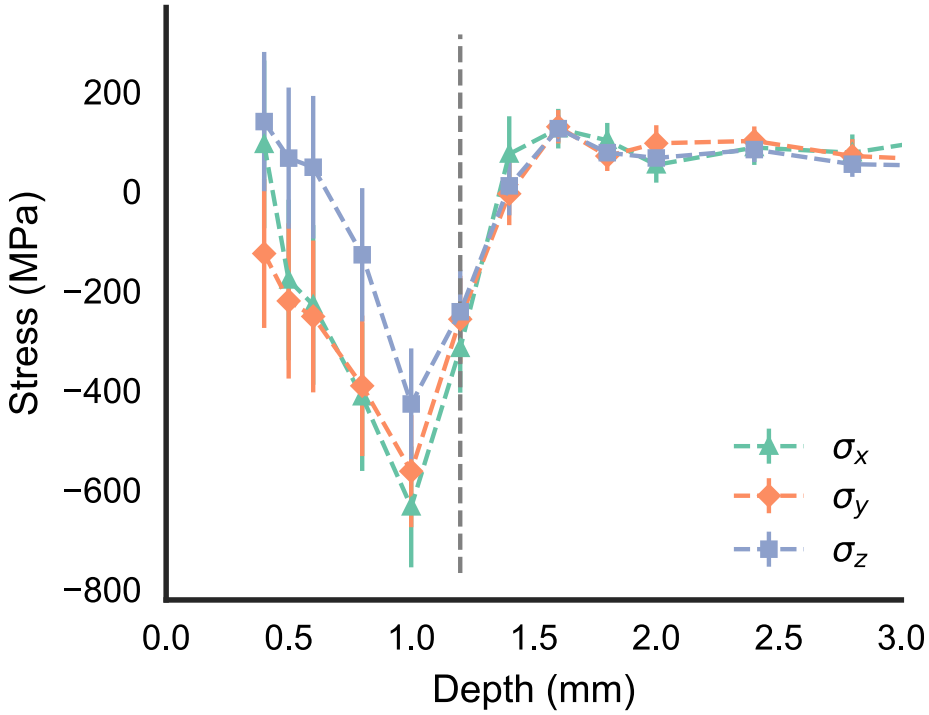

Figure 7 – Calculated residual stresses with respect to depth determined using neutron diffraction on SALSA (directions x, y = in-plane, z=out-of-plane).

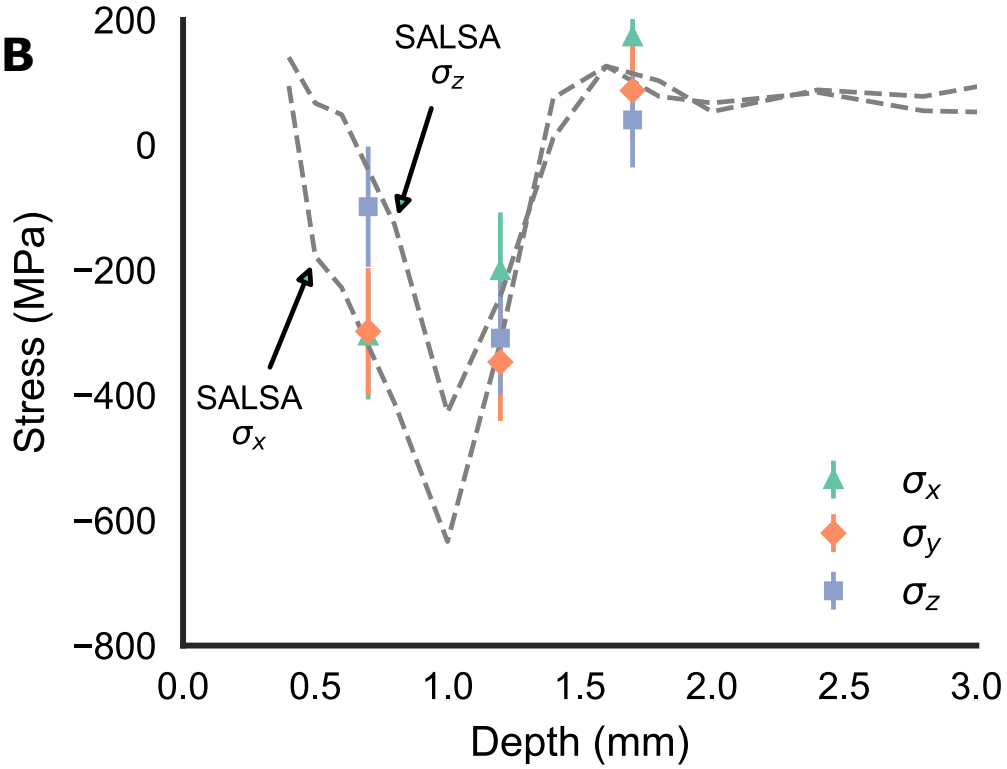

Figure 8 – Calculated as-clad residual stresses from ENGINX and SALSA measurements.

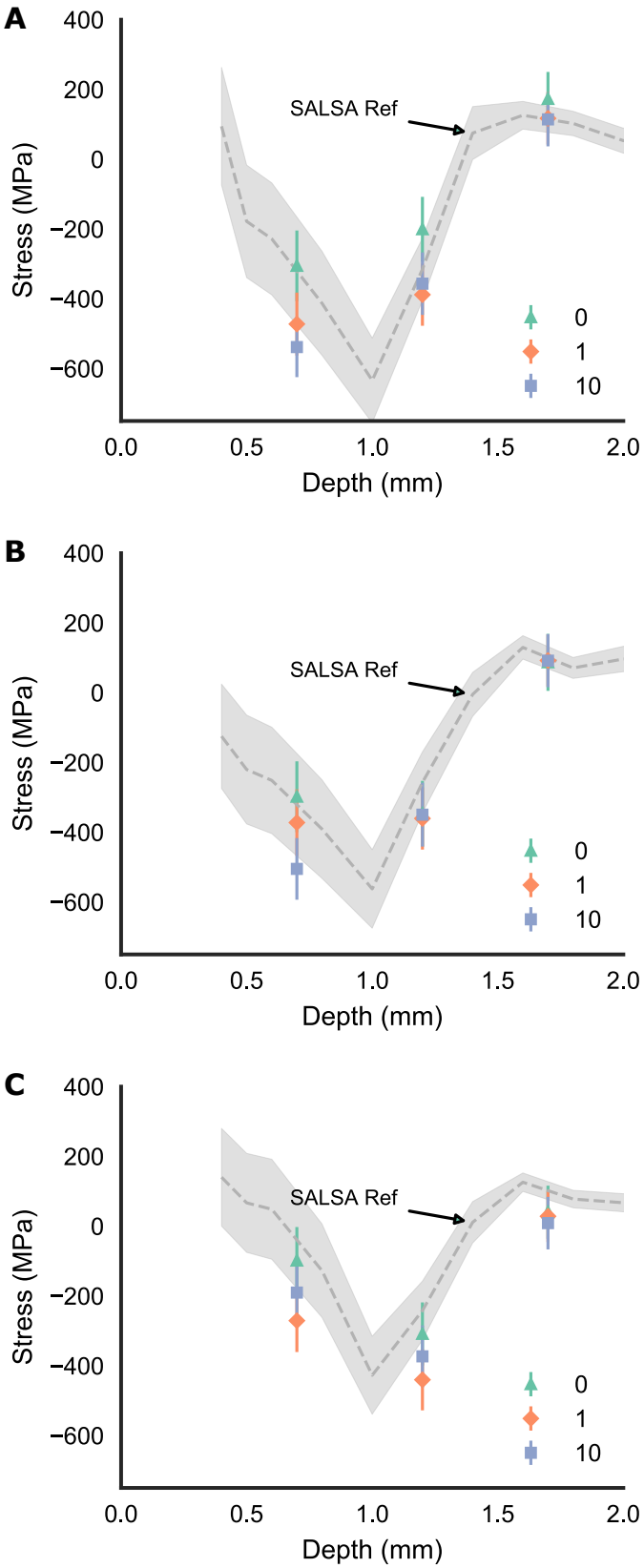

Figure 9 – The effect of applying 4-point bending on the residual stresses in the clad rail in the A) longitudinal (σ_x), B) transverse (σ_y) and C) normal (σ_z) directions. The dotted line with shaded regions represent the nominal stress and uncertainty (1 std) as determined by the SALSA measurements as a reference.

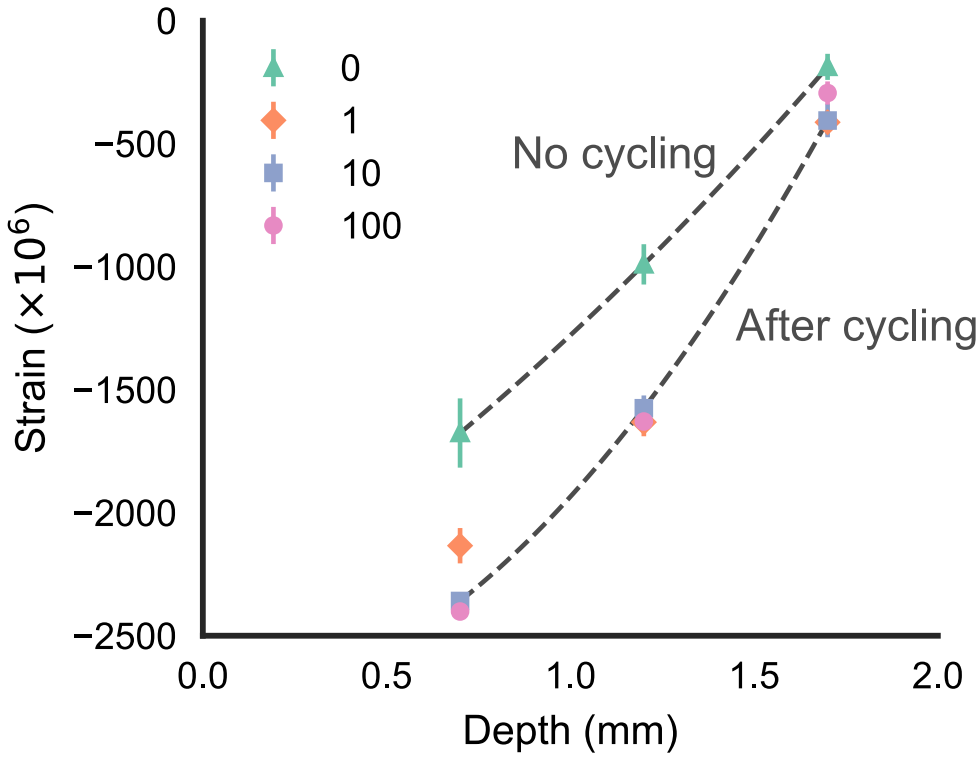

Figure 10 – The longitudinal component of strain in the clad, measured using ENGINX, as a function of applied fatigue cycles. Strain data for 100 cycles was not available in the other two principal directions. The dashed lines are intended to guide the eye.

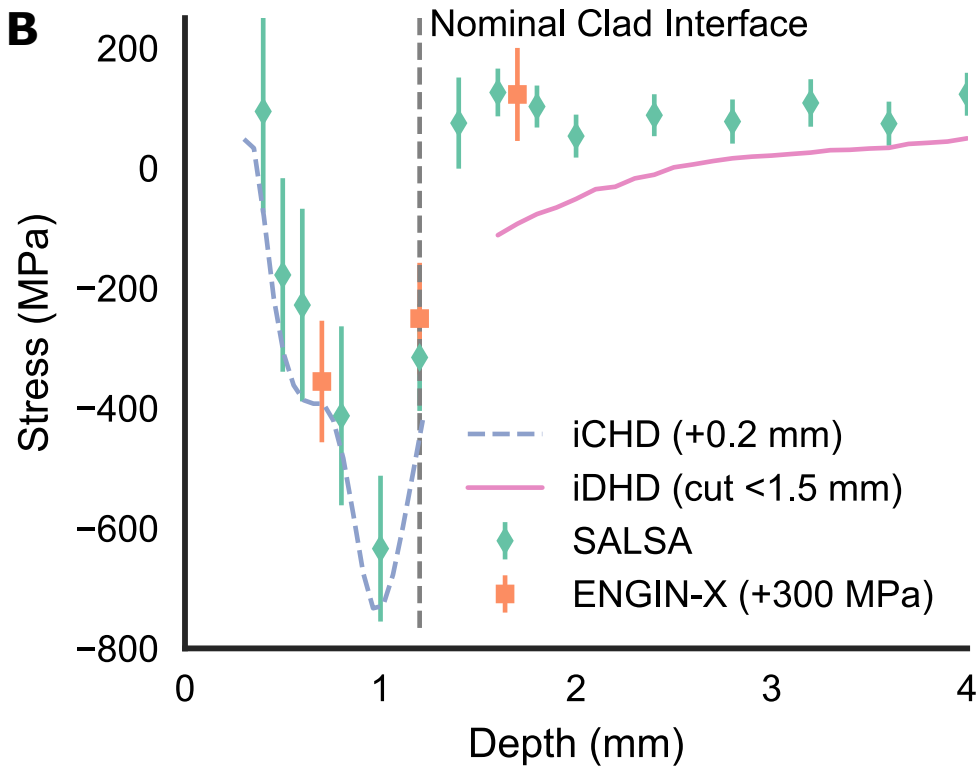

Figure 11 – A comparison of the residual stress in the longitudinal direction of the clad and rail measured using multiple techniques